Increased peak current in AlAs/GaAs resonant tunneling structures with GaInAs emitter spacer

Y. W. Choi and C. R. Wie
State University of New York at Buffalo, Department of Electrical and Computer Engineering and III-V Semiconductor Materials and Devices Laboratory, Bonner Hall, Buffalo, New York 14260

(Received 17 April 1991; accepted for publication 8 November 1991)

Self-consistent simulation results are presented for the symmetric barrier AlAs/GaAs/AlAs resonant tunneling structures with a GaInAs emitter spacer well [Appl. Phys. Lett. **58**, 1077 (1991)]. A simple model is used to handle the two-dimensional emitter accumulation electrons. These accumulation electrons below the emitter launching energy are treated as pseudo three-dimensional electrons, distributed continuously down to a certain minimum energy. With a proper choice of this bottom energy, a good agreement is achieved in the peak position between the simulation results and the experimental data. The best fit value of the bottom energy for the accumulated electrons was about $\frac{2}{3}\Delta E_c$ below the emitter conduction band edges for all diodes. Also, the simulation results could explain the systematic variation of the experimental peak current and voltage values as a function of the GaInAs spacer well depth. In order to provide a design guideline, the layer parameters were systematically varied and the simulation results on the peak current are presented. The peak current density is found to be most sensitive to the AlAs barrier thickness, especially to the emitter barrier thickness, and it is further increased by using an emitter spacer well. Based on our theoretical analyses, a 10-Å AlAs double barrier and 50-Å GaAs well with a 50-Å $Ga_{0.9}In_{0.1}As$ emitter spacer well could produce a peak current density as high as 2200 kA/cm^2.

I. INTRODUCTION

Since the pioneering work of resonant tunneling by Esaki, Tsu, and Chang,[1] many experimental,[2–6] and theoretical[7–16] studies have been conducted on double-barrier resonant tunneling structure (RTS). Interests in RTS were stimulated by the promising potential for high-speed and new functional devices,[17,18] and the desire to understand the electron transport process. Owing to the advanced epitaxial growth technologies, such as molecular beam epitaxy (MBE) and metal-organic chemical vapor deposition, high quality RTS can be made. Recently, pseudomorphic strained layers were incorporated into the structure[3–5] in order to improve the device performance. We have also introduced a simple yet systematic design method for increasing the peak current density by using a strained emitter spacer layer (ESL).[3] Much research work was also devoted to understanding and predicting the current–voltage (I–V) characteristics. The self-consistency in I–V calculation[7–9] is important in a structure with undoped or lightly doped spacer layers because the accumulation and depletion of the electrons in the spacer layers affect the electrostatic potential profile and thereby affect the I–V characteristics. Self-consistently calculated potential profile introduces localized two-dimensional (2D) electrons in the emitter accumulation region. For example, Mounaix *et al.*[10] observed the resonant tunneling from the localized states in the accumulation layer, and Jogai *et al.*[11] pointed out the importance of the localized states for structures with a thick (500 Å), lightly doped spacer layer. If the structure includes an emitter spacer layer with its conduction band edge lower than the emitter conduction band edge, the localized 2D states will be even more important.

In this paper, results from the simulation studies of AlAs/GaAs RTS with a GaInAs ESL are presented. We use, in particular, a self-consistent I–V calculation which is based on Thomas–Fermi (TF) screening approximation.[7,14] In the simulation, we model the two-dimensional states in the spacer well as pseudo three-dimensional states with the energy distributed in continuum. The bottom energy of the accumulated electrons is adjusted to give the closest values to the experimental peak current and voltage. In Sec. II, the experimental procedure is briefly described. In Sec. III, the detailed calculation procedure is presented. In Sec. IV, we discuss the experimental data using the simulation results. In Sec. V, the dependence of peak current density (J_p) and peak voltage (V_p) on the layer parameters are discussed with an objective to optimize the device structure. In Sec. VI, we summarize this work.

II. EXPERIMENT

Samples used in this study were grown by MBE on n^+-GaAs (100) substrates. Figure 1 shows the schematic layer structure and the flat-band band diagram. The indium content of the 50-Å GaInAs layer was varied from 0% to 20% to study the dependence of device characteristics on the spacer well depth. To verify the structural parameters of the strained GaInAs layer, x-ray interference analysis[20] was performed using the conventional double-crystal rocking curve technique. A good fit to the experimental rocking curves by simulated ones was obtained

 © 1992 American Institute of Physics

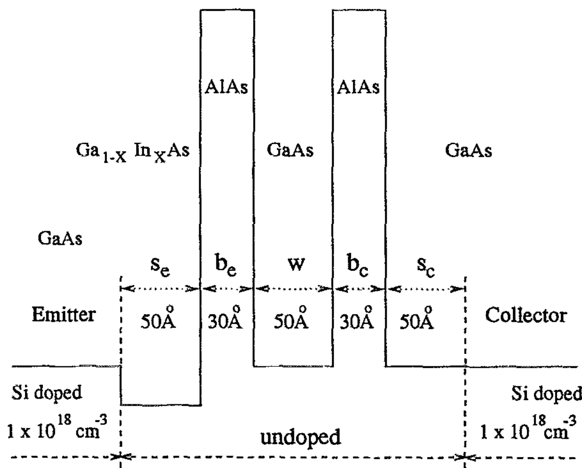

FIG. 1. Schematic illustration of the sample structure with a strained pseudomorphic $Ga_{1-x}In_xAs$ ($x=0$, 0.05, 0.1, 0.15, and 0.2) ESL. The nominal growth parameters of the structure and their nomenclature are shown.

using the nominal growth parameters for all samples with an exception for the $x = 15\%$ sample, for which analysis showed a significant deviation in the actual layer parameters from the nominal growth parameters. Ohmic contacts were made on the front and back sides of the wafer using AuGe/Au metallizations and 420 °C rapid thermal annealing for 30 s. The mesa-etched diodes ranged in area from 28×28 to 36×36 μm^2 defined by wet chemical etching and conventional photolithography. The diode sizes were carefully determined from optical microscope pictures. The *I–V* characteristics were measured with HP 4145B semiconductor parameter analyzer. The bias voltage was swept at a rate of 1 mV/6.5 s. Pseudo four-terminal technique was used to reduce the effect of external resistance.

III. *I–V* CALCULATION

Considering the nonequilibrium feature of the resonant tunneling devices, Frensley[15] and Kluksdahl *et al.*[16] treated the quantum transport using Wigner function representation. Frensley[15] showed that phonon scattering and contact resistivity must be included in the self-consistent calculation in order to achieve a physically acceptable potential profile. However, it was also found that potential profiles obtained by Wigner function calculation including the phonon scattering process and the contact resistivity are quite similar to that obtained using the TF-screening approximation which is essentially an equilibrium model.[15] TF model is probably the simplest self-consistent approximation, where as Wigner function calculation describes the nonequilibrium carrier transport process physically and mathematically more rigorously. As long as electrons are scattered into the accumulation layer much more rapidly than they leave it by tunneling through the barriers, results obtained by TF equilibrium model would closely resemble those obtained by Wigner function calculation.[15] Also, TF model has been used by many researchers to analyze their experimental data[10–13] and to predict the *I–V*

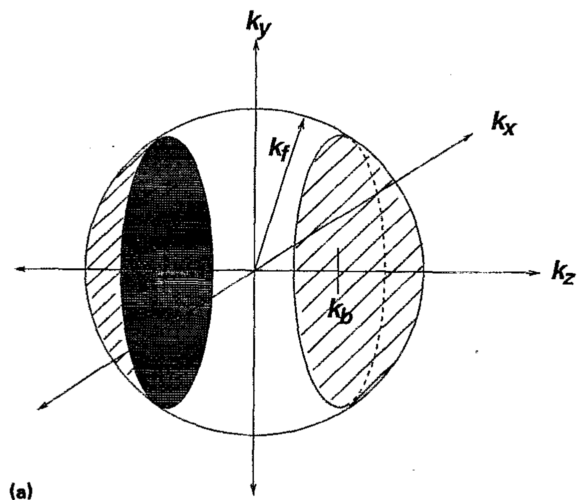

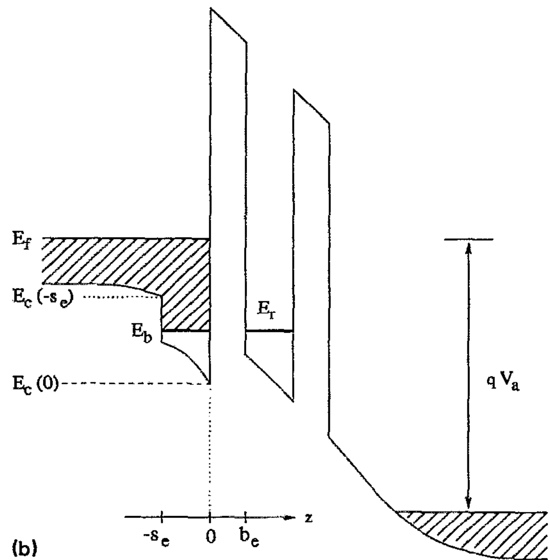

FIG. 2. (a) Fermi sphere at 0 K, and (b) self-consistently calculated potential profile biased at the peak voltage.

characteristics.[14] For example, Reed *et al.*[13] have found a good agreement between the experiments and the calculation using the TF approximation for the precisely characterized resonant tunneling structures. Jogai *et al.*[11] used TF approximation to describe the accumulated electrons confined in the accumulation well by treating them as fully three dimensional with all energy states allowed down to the conduction band edge. If the accumulated electrons are treated as fully three dimensional with all states allowed, their numbers will then be overestimated. This problem will be aggravated if the accumulation layer has a lower conduction band edge than the emitter region, as in our samples. In order to partially avoid this problem, we modeled the accumulation electrons to be continuously distributed to certain bottom energy (E_b) which is higher than the conduction band edge.

Figure 2(a) shows our model Fermi sphere at 0 K, where the dashed volume corresponds to the filled states in the GaInAs accumulation layer shown in Fig. 2(b). The

Fermi sphere is located at $z=0$ in the GaInAs layer. In the TF approximation, the density of 3D electrons at position z in the GaInAs layer can be expressed as

$$n(z)=\frac{k_BT}{4\pi^2}\left(\frac{2m_c^*}{\hbar^2}\right)^{3/2}\times\int_{E_b}^{\infty}dE_l\frac{\ln(1+\exp([E_f-E_l-2E_c(z)]/k_BT))}{\sqrt{E_l-E_c(z)}},\tag{1}$$

where E_b is the energy bottom of the pseudo 3D electrons, E_f is the Fermi energy, $E_c(z)$ is the conduction band edge at position z, and E_l is the longitudinal electron energy in z direction. Note that in Eq. (1), there is a gap between E_b and $E_c(z)$. The potential profile was segmented into 1-Å size and in each segment the potential energy was assumed constant. Above the forward bias of about 0.1 V, the effects of collector-to-emitter flow on the electron density profile and the total current density was negligible. After convergence has been achieved, the current density is calculated using

$$J=\frac{qm_c^*k_BT}{2\pi^2\hbar^3}\int_{E_b}^{\infty}dE_l|T(E_l)|^2\left(\frac{E_l-E_c(0)-qV_a}{E_l-E_c(0)}\right)^{1/2}\times\ln\left(\frac{1+\exp([E_f-E_l-2E_c(0)]/k_BT)}{1+\exp([E_f-E_l-qV_a-2E_c(0)]/k_BT)}\right),\tag{2}$$

where $E_c(0)$ is the conduction band edge at the GaInAs–AlAs interface and is set to zero in the calculation. The transmission coefficient $T(E_l)$ in Eq. (2) was calculated over the whole structure, including the GaInAs spacer layer. However, in the formulation of Eq. (2), $T(E_l)$ may be calculated only for the structure to the right of the GaInAs–AlAs interface [see Fig. 2(b)] because the electron launching position is $z=0$ in our simulation.

In the simulation, we used the nominal growth parameters for the layer thickness and the doping concentration. The effective mass of $Ga_{1-x}In_xAs$ was assumed to be $(0.067-0.044x)m_0$. The conduction-band offset between GaAs and $Ga_{1-x}In_xAs$ was assumed to be $0.6\Delta E_g$. It was assumed that electrons tunnel through the Γ-valley of the barriers. This is based on the recent report[21] that electrons transport through Γ-valleys for structures with the AlAs barrier thickness of 13 monolayers (about 34 Å) and the GaAs well layer thicker than 14 monolayers (about 36 Å). The band nonparabolicity[19,22,23] was considered and the electron effective mass in AlAs barriers was estimated to be $0.10m_0$. Our calculated peak current density obtained using the reduced AlAs effective mass of $0.10m_0$ was much closer to the experimental peak current density and was about four times larger than that obtained using the Γ-point effective mass of $0.15m_0$.

Since the experimental valley current is dominated by currents other than the resonant tunneling current through the Γ-barrier, the TF model calculation cannot account for the valley current (actually vastly underestimates it). The comparison with the experimental peak current values was done using the calculation with a decreasing bias, because the calculation with an increasing bias caused intrinsic bistability due to the electrostatic feedback effect.[14]

IV. SIMULATION ANALYSIS OF EXPERIMENTAL DATA

The bottom energy in the GaInAs layer was adjusted until a reasonable agreement was obtained between the simulated and experimental values of J_p and V_p. Using the bottom energy of about $\frac{2}{3}\Delta E_c$ below the GaAs emitter conduction band edge (at the GaAs–GaInAs interface) resulted in a good agreement for all diodes of different GaInAs compositions except for the 15% indium, where ΔE_c is the conduction-band offset between GaAs and GaInAs. Using the pseudo 3D states fully filled down to the conduction band edge $E_c(0)$, the simulated peak voltage was about 2 times larger than the experimental peak voltage. This indicates that the fully-filled emitter spacer well is not the true picture.

Consider the bound-state energy level and the energy uncertainty due to the finite thickness of the GaInAs well. The calculated energy level at zero bias is 12.7, 37.1, and 65.6 meV below the GaAs conduction-band edge for $x=10\%$, 15%, and 20% samples, respectively. No bound state exists in the 5% sample. The energy uncertainty $(\hbar^2/2m^*s_e^2)$ is about 25 meV in the 50-Å GaInAs well. It is interesting to note that $\frac{2}{3}\Delta E_c$ corresponds roughly to 25 meV (the energy uncertainty) below the energy levels in the GaInAs well.

Figure 3 shows the experimental and simulated I–V curves. The peak voltage and current values are listed in Table I. As the indium composition increases, increases in the J_p and V_p values are clearly seen in both the experimental and calculated results. The simulated value of J_p rather than J_p-J_v (Ref. 19) was compared with the experimental peak current density because the experimental peak current density did not change significantly with decreasing the temperature whereas the valley current decreased substantially. The experimental V_p was adjusted for an I_pR_s voltage drop ($V_p'=V_p-I_pR_s$). The series resistance (R_s), estimated from the slope of experimental I–V curves at 2 V, was about 1.45 Ω for a 28×28-μm^2 sample. The calculated peak voltages for the $x=5\%$ and 10% diodes are slightly less than the experimental V_p'. The reverse bias peak voltages of the 5% and 10% diodes are also larger than those of the 0% and 20% samples. Therefore, the discrepancy in the peak voltage for the $x=5\%$ and $x=10\%$ diodes is believed to be due to a smaller GaAs well thickness than the nominal thickness of 50 Å. Calculations with a GaAs well thickness of 47 Å for the 5% and 10% samples gave a much better agreement with the experimental data. The good agreement between the experimental data and the calculated values justify our physical picture and simulation approach as represented by Fig. 2 and Eqs. (1) and (2) for handling the accumulated electrons in the GaInAs emitter spacer well.

The potential profiles for the $x=0\%$, 10%, and 20% diodes biased at the peak voltage of the 10% diode, are shown in Fig. 4. It can be seen that a higher bias voltage is

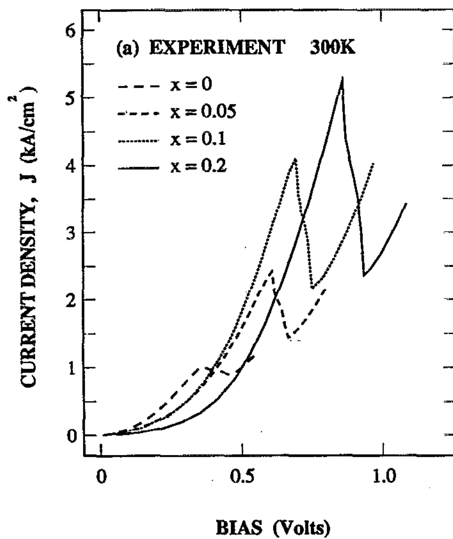

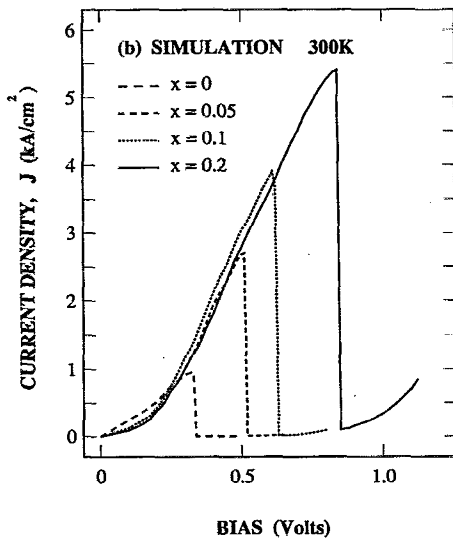

FIG. 3. (a) Experimental and (b) simulated I–V curves. Voltage sweep for the simulated curves was from high to low voltage to exclude any electrostatic feedback effect.

needed to achieve the current peak for a sample with a higher indium content. At a given bias, the resonant tunneling current will be approximately determined by the integrated transmission probability, which is $|T(E_l)|^2$ in-

TABLE I. Lists of peak voltages V_p (volts) and current densities J_p (kA/cm^2) obtained by experiment and simulation at 300 K. External series resistance (R_s) is assumed to be 1.45 Ω. Simulation peak voltages are for voltage sweeping from high to low.

Indium composition (%)	Experiment			Simulation	
	V_p	J_p	$V_p - I_p R_s$	V_p	J_p
0	0.36	1.01	0.32	0.33	0.95
5	0.62	2.42	0.58	0.51	2.73
10	0.70	4.10	0.66	0.61	3.96
15	0.66	2.86	0.61	0.72	4.50
20	0.86	5.25	0.80	0.84	5.38

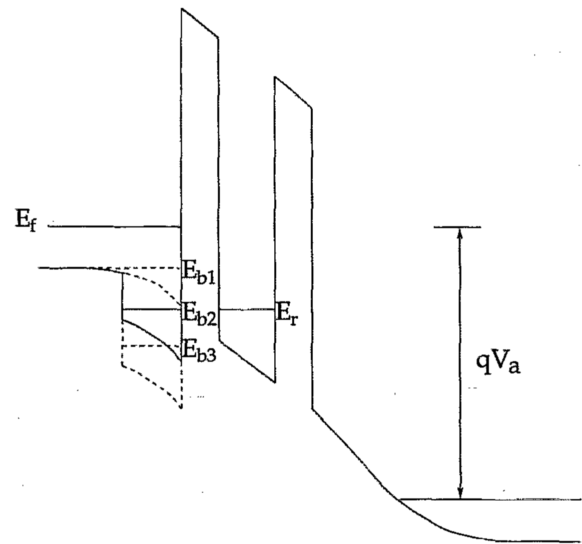

FIG. 4. Potential profiles for different ESL indium composition ($x = 0$, 0.1, and 0.2) biased at the peak voltage of the $x = 0.1$ sample.

tegrated over the longitudinal electron energy E_l centered around E_r, multiplied by the number of resonant electrons (N_r). N_r is proportional to the area at $k_z = \sqrt{2m^* E_l/\hbar^2}$ in the Fermi sphere shown in Fig. 2(a). Figure 5 shows the transmission probability integrated over longitudinal energy, $\int_0^{E_{\min 1}} |T(E_l)|^2 \, dE_l$, as a function of the applied bias voltage V_a. Here $E_{\min 1}$ is the energy at the minimum of $|T(E_l)|^2$ between the first and second energy levels of the GaAs well. For a given GaInAs composition, it can be seen that the integrated transmission probability decreases as the applied bias is increased. At the peak voltage, however, which is indicated by the filled circles in Fig. 5, the integrated transmission probability is approximately the same for all the different samples. This suggests that the peak current of our diodes is controlled by the number of resonant electrons at the peak voltage. This result demonstrates that given the double barrier structure, use of an emitter spacer well increases the number of resonant electrons at the peak voltage and a deeper emitter spacer well will give more resonant electrons at the peak voltage. This

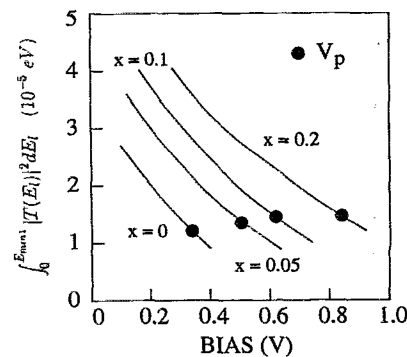

FIG. 5. $\int_0^{E_{\min 1}} |T(E_l)|^2 \, dE_l$ vs applied bias (V_a) plot. The filled circles are the integrated transmission probability at the peak voltages.

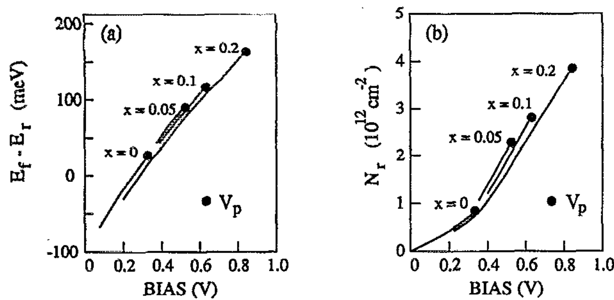

FIG. 6. $E_f - E_r$ vs V_a plot (a) and the number of resonant tunneling electron N_r vs V_a plot (b). The filled circles are for the peak voltages.

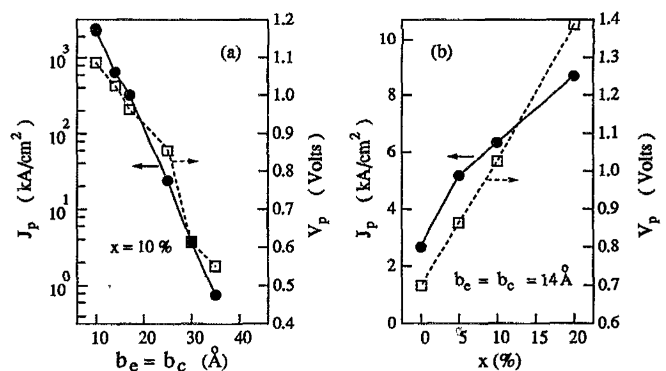

FIG. 7. Simulated J_p and V_p as a function of (a) emitter and collector barrier thickness, $b_e = b_c$ and (b) indium composition of ESL.

is a simple and practical design tool which can be used to further increase the peak current density (and the peak to valley ratio[3]) of a structurally optimized double barrier single well structure.

In Fig. 6, the number of resonant tunneling electrons N_r and the quasistationary ground-state energy level E_r are shown as a function of applied bias. Increases in the N_r and $E_f - E_r$ are seen, as expected, with the increase in the bias voltage. Note that at a given bias, N_r and $E_f - E_r$ do not show any substantial dependence on the emitter spacer well depth, as can be seen from the indium-composition dependence in Fig. 6. The increased peak current density is concomitant with the increased peak bias voltage, as can be seen in Figs. 3 and 6. Therefore, our I–V data for devices with an emitter spacer well are reasonably well described by a model using pseudo 3D electrons in the GaInAs emitter spacer layer.

V. DEPENDENCE OF PEAK CURRENT AND VOLTAGE ON LAYER PARAMETERS

The design objective may be the achievement of a highest possible peak current density at a lowest possible peak voltage with a high peak-to-valley ratio and a wide valley region. Using the simulation method, presented in the previous section, the dependence of peak current and voltage on the layer parameters was investigated. Using this simulation method, however, the valley current could not be studied because, as can be seen from the comparison of Figs. 3(a) and 3(b), the valley current in real devices are dominated by the transport mechanisms other than the resonant tunneling through the Γ-valley barrier. In order to show the effects on the current peak, the layer parameters (thickness and potential height) were systematically varied. Simulation results are presented for devices based on a GaAs substrate. It should be pointed out that we have not considered the effects of other physical parameters, such as the effects of interface roughness, alloy scattering, and phonon scattering, because it is beyond the scope of this paper.

J_p is increased exponentially with the decrease of the barrier thickness, as expected from the simple quantum mechanics of tunneling, and is shown for the $x = 10\%$ sample in Fig. 7(a). Hereafter, other unmentioned layer parameters are the same as those given in Fig. 1. With the barrier thickness of $b_e = b_c = 10$ Å, a peak current density of 2200 kA/cm^2 is found from our simulation for the $x = 20\%$ sample. Recently, a J_p value over 250 kA/cm^2 was reported by Wolak *et al.*[19] using a 14-Å AlAs barrier and 51-Å GaAs QW. Figure 7(b) shows that J_p is 275 kA/cm^2 for a 14-Å barrier and 50-Å QW for zero indium in the GaInAs emitter spacer, showing a good agreement with the data by Wolak *et al.* Figure 7(b) also shows the dependence of J_p and V_p on the indium content in the GaInAs emitter spacer layer. For the structure with $b_e = b_c = 14$ Å and $x = 20\%$, the simulated J_p is 870 kA/cm^2. Calculation shows that V_p is increased with decreasing the barrier thickness because of the larger transmission coefficient which also increases the trapped charge in the QW. Figure 8 shows that the increased trapped charge electrostatically moves the QW conduction band edge upward.

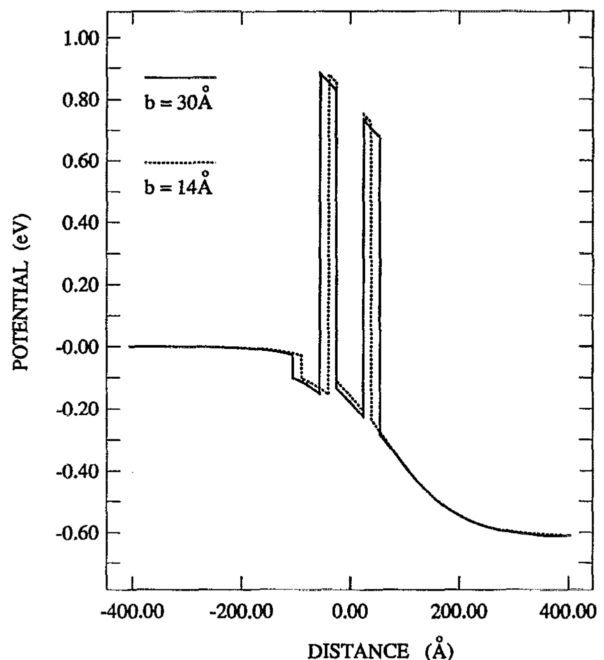

FIG. 8. Potential profiles of the structures with 30-Å AlAs barrier (solid line) and 14-Å barrier (dotted line) biased at 0.61 V. Higher QW potential of the thinner barrier structure is shown while the bottom energy of pseudo 3D electron in ESL is almost the same.

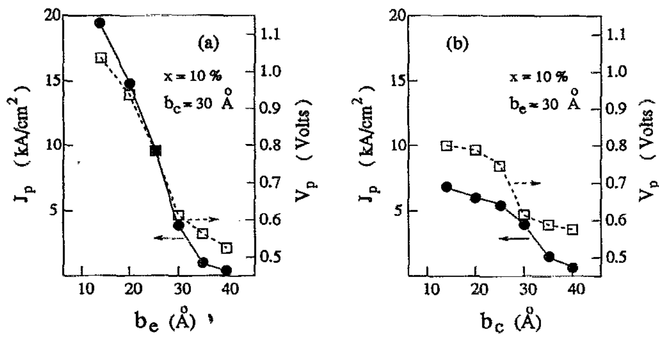

FIG. 9. Simulated J_p and V_p as a function of (a) the emitter barrier thickness, b_e and (b) the collector barrier thickness, b_c.

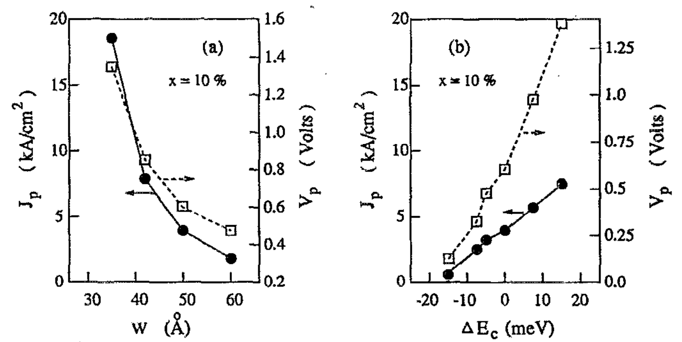

FIG. 11. Simulated J_p and V_p as a function of (a) QW thickness and (b) QW depth ΔE_c. For the positive ΔE_c, we used an AlGaAs QW, while we used GaInAs QW for negative ΔE_c.

Figure 9 shows the dependences of J_p and V_p on the emitter (b_e) and collector (b_c) barrier thicknesses. It can be seen that b_e controls J_p and V_p much more effectively than b_c. This is because the global transmission coefficient and the amount of trapped charge in the QW are affected more strongly by the change in b_e than the change in b_c.[24] In summary, Figs. 7(a), 8, and 9 show the effect of AlAs barrier thickness on the current peak of GaAs-based RTS, and Fig. 7(b) shows the effect of the depth of emitter spacer well for a 14-Å-thick AlAs barrier RTS.

Figure 10 shows the effect of the changing bottom energy E_b in the GaInAs emitter spacer layer (note that E_b is related with the thickness s_e). As E_b is lowered, only a slight increase in the J_p is seen even though, for example, N_r at V_p increases by about 20% as the E_b is lowered from $E_c(-s_e) - 30$ meV to $E_c(-s_e) - 50$ meV. The decreased transmission coefficient at the higher peak bias, however, causes an insignificant increase in J_p. On the other hand, V_p increases more significantly as E_b is lowered. A 20 meV lowering in E_b results in about 70 meV increase in V_p. Figure 11(a) shows the effect of changing GaAs QW thickness. As the GaAs QW thickness is increased from 35 to 60 Å, J_p is decreased from 18.7 kA/cm^2 to 1.94 kA/cm^2 and V_p from 1.35 to 0.47 V. The substantial decrease in J_p and V_p as the QW widens is probably due to the decreased integrated transmission probability from

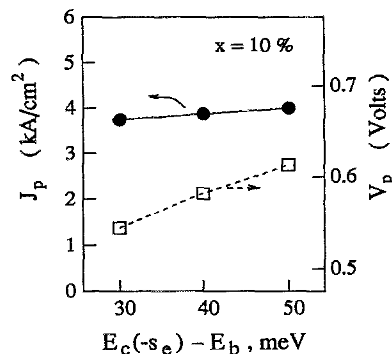

FIG. 10. Simulated J_p and V_p as a function of the bottom energy of pseudo 3D electrons, $E_c(-s_e) - E_b$.

the fact that the lowering of E_r causes the sharpening of the transmission coefficient around the resonance peak.[25]

In order to see the dependence of peak current and voltage on the QW depth for a given RTS (the same as Fig. 1 except the well layer), we used GaInAs for wells deeper and AlGaAs for wells shallower than the GaAs well. Here, the effect of alloy scattering due to the ternary alloy composition was not included in the simulation because our primary interest was to find the qualitative trend and a rough order of magnitude change in J_p and V_p due to the varying well depth. Figure 11(b) shows the dependence. As can be seen from the figure, when the 50-Å GaAs well is replaced by a 50-Å $Ga_{0.8}In_{0.2}As$ well (change in well bottom is -15 meV), the J_p and V_p are reduced from 3.96 kA/cm^2 and 0.61 V to 0.55 kA/cm^2 and 0.12 V, respectively. It can be seen that as the 50-Å GaAs well is replaced by a 50-Å $Al_{0.2}Ga_{0.8}As$ (change in well bottom is $+15.7$ meV), both the J_p and V_p are increased roughly by a factor of two. The peak current is reduced for the GaInAs well. It has been reported, however, that the device with a GaInAs QW can show a high peak-to-valley ratio due to the reduced valley current,[26] which, in turn, may be due to a larger separation between the first energy level and the second level in the well. However, as was mentioned already, our $I-V$ simulation using the TF model could not predict the valley current and thus the peak-to-valley ratio. The Wigner function approach, which incorporates the scattering processes into the simulation, will be more appropriate for studying the valley current and the peak-to-valley ratio.

VI. SUMMARY

Simulation results based on TF equilibrium model were presented to more fully understand the systematic increases in peak current density and peak voltage in AlAs/GaAs/AlAs resonant tunneling diodes with a pseudomorphic strained GaInAs emitter spacer layer of varying composition. In the simulation, the two-dimensional accumulation electrons in the GaInAs emitter spacer well was treated as pseudo three-dimensional electrons, distributed down to a certain minimum energy. With the bottom energy of the pseudo three-dimensional elec-

trons about $\frac{2}{3}\Delta E_c$ below the GaAs emitter conduction band edge, a good agreement in the peak current and peak voltage was achieved between the simulated I–V curves and the experimental data. From the simulation, the effects of thickness and conduction band edge of each layer on the peak current value were presented. It was shown that the peak current density can be further increased by employing an emitter spacer well layer. Based on our simulation, a peak current density up to 2200 kA/cm^2 was obtained when we used 10-Å AlAs barriers, a 50-Å GaAs well, and a 50-Å $Ga_{0.9}In_{0.1}As$ emitter spacer layer.

ACKNOWLEDGMENTS

This work was supported in part by the National Science Foundation under Grants No. ECS-8913229 and No. DMR-8857403. The authors acknowledge the x-ray analysis by H. M. Kim and the MBE growth by Professor Gary W. Wicks group at University of Rochester. One of us (C.R.W.) is a National Science Foundation Presidential Young Investigator.

[1] L. Esaki and R. Tsu, IBM J. Res. Dev. **14**, 61 (1970); L. L. Chang, L. Esaki, and R. Tsu, Appl. Phys. Lett. **24**, 593 (1974).
[2] A. R. Bonnefei, T. C. McGill, R. D. Burnham, and G. B. Anderson, Appl. Phys. Lett. **50**, 344 (1987).
[3] C. R. Wie and Y. W. Choi, Appl. Phys. Lett. **58**, 1077 (1991).
[4] T. P. E. Broekaert, W. Lee, and C. G. Fonstad, Appl. Phys. Lett. **53**, 1545 (1988); T. P. E. Broekaert and C. G. Fonstad, J. Appl. Phys. **68**, 4310 (1990).
[5] R. Kapre, A. Madhukaar, K. Kaviani, S. Guha, and K. C. Rajkumar, Appl. Phys. Lett. **56**, 922 (1990).
[6] P. Cheng and J. S. Harris, Jr., Appl. Phys. Lett. **56**, 1676 (1990).
[7] H. Ohnishi, T. Inata, S. Muto, N. Yokoyama, and A. Shibatomi, Appl. Phys. Lett. **24**, 1248 (1986).
[8] M. Cahay, M. McLennan, S. Datta, and M. S. Lundstrom, Appl. Phys. Lett. **50**, 612 (1987).
[9] W. Pötz, J. Appl. Phys. **66**, 2458 (1989).
[10] P. Mounaix, O. Vanbesien, and D. Lippens, Appl. Phys. Lett. **57**, 1517 (1990).
[11] B. Jogai, C. I. Huang, and C. A. Bozada, J. Appl. Phys. **66**, 3126 (1989); B. Jogai, C. I. Huang, E. T. Koenig, and C. A. Bozada, J. Vac. Sci. Technol. B **9**, 143 (1991).
[12] E. T. Koenig, C. I. Huang, and B. Jogai, J. Appl. Phys. **68**, 5905 (1990).
[13] M. A. Reed, W. R. Frensley, W. M. Duncan, R. J. Matyi, A. C. Seabaugh, and H.-L. Tsai, Appl. Phys. Lett. **54**, 1256 (1989).
[14] R. K. Mains, J. P. Sun, and G. I. Haddad, Appl. Phys. Lett. **55**, 371 (1989).
[15] W. R. Frensley, Solid-State Electron. **32**, 1235 (1989).
[16] N. C. Kluksdahl, A. M. Kriman, D. K. Ferry, and C. Ringhofer, Phys. Rev. B **39**, 7720 (1989).
[17] T. C. L. G. Sollner, W. D. Goodhue, P. E. Tannenwald, C. D. Parker, and D. D. Peck, Appl. Phys. Lett. **43**, 588 (1983).
[18] F. Capasso, S. Sen, A. Y. Cho, and D. L. Sivco, Appl. Phys. Lett. **53**, 1056 (1988); N. Yokoyama, K. Imamura, S. Muto, S. Hiyamizu, and H. Nishi, Jpn. J. Appl. Phys. **24**, L853 (1985).
[19] E. Wolak, E. Özbay, B. G. Park, S. K. Diamond, D. M. Bloom, and J. S. Harris, Jr., J. Appl. Phys. **69**, 3345 (1991).
[20] C. R. Wie, J. C. Chen, H. M. Kim, P. L. Liu, Y. W. Choi, and D. M. Hwang, Appl. Phys. Lett. **55**, 1774 (1989); C. R. Wie, J. Appl. Phys. **65**, 1036 (1989).
[21] D. Z.-Y. Ting, M. K. Jackson, D. H. Chow, J. R. Söderström, D. A. Collins, and T. C. McGill, Solid-State Electron. **32**, 1513 (1989); D. Z.-Y. Ting and T. C. McGill, J. Vac. Sci. Technol. B **7**, 1013 (1989).
[22] N. Schulman and Y.-C. Chang, Phys. Rev. B **24**, 4445 (1981).
[23] S. Muto, T. Inata, Y. Sugiyama, Y. Nakata, T. Fujii, H. Ohnishi, and S. Hiyamizu, Jpn. J. Appl. Phys. **26**, L244 (1987).
[24] B. Ricco and M. Ya. Azbel, Phys. Rev. B **29**, 1970 (1984).
[25] M. Tsuchiya and H. Sakaki, Appl. Phys. Lett. **49**, 88 (1986).
[26] H. Toyoshima, Y. Ando, A. Okamoto, and T. Itoh, Jpn. J. Appl. Phys. **25**, L786 (1986).

Journal of Applied Physics is copyrighted by the American Institute of Physics (AIP). Redistribution of journal material is subject to the AIP online journal license and/or AIP copyright. For more information, see http://ojps.aip.org/japo/japcr/jsp
Copyright of Journal of Applied Physics is the property of American Institute of Physics and its content may not be copied or emailed to multiple sites or posted to a listserv without the copyright holder's express written permission. However, users may print, download, or email articles for individual use.

Journal of Applied Physics is copyrighted by the American Institute of Physics (AIP). Redistribution of journal material is subject to the AIP online journal license and/or AIP copyright. For more information, see http://ojps.aip.org/japo/japcr/jsp